Investigation of basic imaging properties in digital radiography. 5. Characteristic curves of II–TV digital systems[a)]

Hiroshi Fujita, Kunio Doi, Maryellen Lissak Giger, and Heang-Ping Chan
Kurt Rossmann Laboratories for Radiologic Image Research, Department of Radiology, The University of Chicago, Chicago, Illinois 60637

(Received 8 February 1985; accepted for publication 4 November 1985)

A simple method was devised to determine the characteristic curve of image intensifier (II)–TV digital imaging systems, which relates the output pixel value to the input relative x-ray intensity. To provide a wide range of x-ray intensities incident on the II, we used an aluminum stepwedge consisting of nine steps with thickness increments of 6.3 mm, together with an 0.81-mm-thick copper plate. The x-ray field was narrowly collimated to the area occupied by the stepwedge in order to reduce the effect of veiling glare. The relative x-ray intensities transmitted through each step of the stepwedge were determined by using screen–film systems. The gradient curve of the system was derived from the slope of the characteristic curve. Results obtained with a Siemens Digitron 2 system showed that its characteristic and gradient curves depended upon the matrix size used, but did not change with the II field size. The validity of the characteristic curve was demonstrated by measurement of iodine attenuation curves obtained with the II–TV digital system at different exposure levels.

Key words: digital radiography, image quality, II–TV system

I. INTRODUCTION

Characteristic (or H&D) curves have been used extensively with conventional film and screen–film recording systems. Such curves are useful in the comparison of system speeds and in the linearization of the system response for measurement of the modulation transfer function (MTF) and other physical quantities.[1–3] At present, several different methods for determining the characteristic curve of screen–film systems are available.[4–9]

A number of new digital radiographic imaging systems are currently being developed,[10–12] and digital subtraction angiography (DSA) systems[11–14] in particular have been successfully used in clinical practice. The characteristic curve of a digital radiographic imaging system can be defined, in a way similar to that of a screen–film system, as the relationship of the output in terms of pixel value to the input in terms of relative x-ray intensity. The characteristic curves of digital imaging systems will be useful for monitoring and comparison of the system response, and also for quantitative analysis[15–17] of digital image information. For example, accurate measurements of basic imaging properties, such as the MTF, cannot be made without knowledge of the characteristic curve. Barnes *et al.* determined the curve for a Picker digital chest unit.[18] MacIntyre *et al.*,[19] Cohen *et al.*,[20] and Seibert *et al.*[21] determined the characteristic curve for a DSA or image intensifier (II)–TV digital unit by making a series of exposures to the II–TV system. However, it is generally difficult to measure the characteristic curve of a DSA unit, because most clinical units are equipped with an automatic exposure control system, and because the flexibility of that system in selecting exposure parameters is limited. In this study, we developed a simple and practical method for determining the characteristic curve of an II–TV (DSA) digital imaging system by using an aluminum stepwedge and a narrow beam.

II. EXPERIMENTAL METHODS

In our study, a Siemens Digitron 2 DSA system was employed as an II–TV digital imaging system. This system includes a Garantix 1000 x-ray generator with a 0.6-mm focal spot x-ray tube, a triple-mode (25, 17, and 12 cm) Optilux RBV 25/17 HN image intensifier with grid (12:1, 40 lines/cm), and a Videomed N TV system. The Digitron 2 contains a 20-megabyte semiconductor memory for image acquisition and storage, and a 10-bit analog-to-digital (A/D) converter with a conversion rate of 20 MHz. Logarithmic or linear amplification is performed prior to A/D conversion. Matrix sizes of 256 × 256 and 512 × 512 are available, and images can be acquired in either a pulsed or a continuous x-ray exposure mode. A Winchester disk of 80 megabytes is used for image storage.

For measurements of the characteristic curve, one can vary the x-ray intensity incident on the II by changing (1) the distance between the focal spot of the x-ray tube and the II, (2) the tube current, or (3) the thickness of an attenuating material. However, because of the automatic exposure control in many DSA systems, manual selection of the tube potential, the tube current, and/or the exposure time may not be possible. In addition, the adjustable distance between the focal spot and the II may not cover the wide range of x-ray intensities required for measurement of the characteristic curve. Therefore, we employed the third method, varying the x-ray intensity by using an aluminum stepwedge as an x-ray beam attenuator. One advantage of this method is that the characteristic curve can be measured from a single image. We determined the x-ray transmission through each

 0094-2405/86/010013-06$01.20

step of the stepwedge by using screen–film systems, as will be described in detail in Sec. V.

The aluminum (type 1100) stepwedge consisted of nine steps, each of which was 1.0 cm × 2.0 cm in area, with thickness increments of 6.3 mm. This stepwedge was used together with a 0.81-mm-thick copper plate, which was placed in front of the II surface (before the grid), in an effort to harden the x-ray beam and to minimize the variation in beam quality through different steps of the stepwedge. The copper plate may also reduce the scattered radiation from the aluminum stepwedge.[22] The distance between the II and the x-ray tube focal spot was 90 cm, and the stepwedge was placed approximately 15 cm from the II.

A problem with the stepwedge method is the presence of veiling glare,[17,21,23–25] which is mainly caused by scattering of x rays, electrons, and light in the II. When the stepwedge is exposed with a broad beam, an approximately constant amount of the veiling glare from the entire II field is added to the stepwedge image; thus the veiling-glare fraction, which is defined as the ratio of the veiling-glare component to the total light output level of the II, in the region of the thick aluminum steps will be greater than that in the thin steps. This implies that the pixel values corresponding to the thick parts of the stepwedge will represent mainly the veiling glare, but not the low-level x-ray intensities incident on the II. In order to reduce this effect of veiling glare, we narrowly collimated the x-ray field to the area occupied by the stepwedge, and thus the contribution of the veiling glare coming from outside the region of the stepwedge was assumed to be negligibly small. Only small amounts of veiling glare generated from each step itself and from neighboring steps will be included in the stepwedge image. This assumption was verified in measurements of attenuation curves of an iodine phantom, as will be discussed later.

For an ideal condition, such as a case in which the x-ray tube current can be varied over a wide range without changing other parameters, the characteristic curve should and could be measured together with the veiling glare, the amount of which is proportional to the x-ray intensity incident on the II.[21] If the veiling glare is eliminated entirely, or if the veiling-glare fraction is constant at all steps of the stepwedge, the corresponding characteristic curves will merely be shifted laterally on the logarithmic relative x-ray intensity axis, and thus the shapes of the curves will remain unchanged. This is the basis of our approach to devise a simple and practical method of measuring the characteristic curve of DSA systems by using the aluminum stepwedge with a narrow-beam geometry.

In order to obtain the stepwedge image with a narrow-beam geometry, one may need to "fool" the automatic exposure control of the DSA system, because the narrow-beam geometry may cause an abnormally high kV setting. For example, a broad-beam exposure may be made initially; then, after the adjustment of the exposure parameters and iris setting is completed by the automatic exposure control in the beginning frames, the exposure field can be collimated down to the desired size while the exposure factors remain unchanged. Instead of the collimator adjustment, an x-ray beam attenuator can be introduced in or removed from the exposure field to "fool" the automatic exposure control so that various exposure factors can be selected, as will be discussed later for measurements of iodine attenuation curves.

III. THE GRADIENT AND ITS APPLICATION TO IMAGE ANALYSIS

The slope of the characteristic curve of a screen–film system, called the gradient, has been used frequently for the evaluation of image contrast.[26] A similar gradient for the II–TV digital system, G, can be defined by

$$G = \left| \frac{\Delta \text{ DSA } \#}{\Delta \log_{10} E} \right|, \tag{1}$$

which is the difference in the DSA pixel values (Δ DSA #) divided by the difference in the log relative x-ray intensities ($\Delta \log_{10} E$). The term Δ DSA # may be regarded as the magnitude of a DSA signal above the background. The absolute value is used because the characteristic curve of our system has a negative slope. In this study, we determined the gradient from the slope of the polynomial-fitted characteristic curve, and we plotted the values versus the DSA pixel value (or DSA number) of the background. From Eq. (1), we can derive the following relationship:

$$\Delta \text{ DSA } \# = -(\log_{10} e)\, G \frac{\Delta E}{E}, \tag{2}$$

which relates the magnitude of the DSA signal, Δ DSA #, to the radiation contrast, $\Delta E/E$, that is equal to the ratio of the signal component ΔE to the background E expressed in terms of the relative x-ray intensities detected by the II. Scattered radiation may be included in the background E. It should be noted that Eq. (2) is applicable only when the veiling glare is negligibly small, or when the veiling-glare fraction in the background region is equal to that in the signal region, since this is the condition under which the characteristic curve is determined. The latter condition arises, for example, when a relatively large object is imaged with a uniform background, i.e., when the object size is much larger than the "size" of the point spread function (PSF) of the veiling glare.[21] However, in clinical imaging situations these conditions usually are not satisfied, and the presence of an almost constant amount of veiling glare reduces the image contrast to less than that estimated from Eq. (2).

In addition, it is generally more important in DSA images to visualize small rather than large objects. When the size of a small, low-contrast object is much less than the size of the PSF of the veiling glare, the amount of veiling glare superimposed on the signal component can be regarded as identical to that on the background adjacent to the signal, and thus the image contrast is reduced in a way similar to the effect of the scattered radiation. Therefore, Eq. (2) has to be modified to include the veiling glare and the scattered radiation, namely,

$$\Delta \text{ DSA } \# = -(\log_{10} e) G \frac{\Delta E}{E_p}(1-s)(1-k). \tag{3}$$

Here, $\Delta E/E_p$ is the "primary" radiation contrast of a small signal, which corresponds to the radiation contrast detected by the II, but without the scattered radiation and veiling glare; s is the scatter fraction, which equals the ratio of the

scattered radiation to the total radiation detected by the II; and k is the veiling-glare fraction, as defined earlier. The veiling-glare fraction can be measured with a lead-disk method, which involves extrapolation to an infinitesimally small disk size.[27]

In a more general situation, in which the object size may not be regarded as small and the background may not be assumed to be uniform, it is likely that the amount of veiling glare varies over the region of the signal and surrounding background, and thus the image contrast cannot simply be determined from Eq. (2) or (3). In such a case, the effect of veiling glare on the signal contrast is complicated and needs to be evaluated by convolution of the PSF of the veiling glare with the spatial distribution of the input x-ray image detected by the II. The spatial distribution of this resulting image in terms of the light output of the II is subsequently converted to that in terms of DSA pixel values by means of a characteristic curve, which can be measured with the method described in this study.

In the determination of the noise Wiener spectrum of the DSA system, the measured Wiener spectrum expressed in terms of DSA pixel values may be converted to that in terms of relative x-ray intensity.[28] One can accomplish this by dividing the measured spectrum by the factor $G^2(1-k)^2(\log_{10} e)^2$, where G is the system's gradient at the average DSA pixel value of the noise pattern, and k corresponds to the veiling-glare fraction measured with a broad-beam exposure. It is assumed that the constant amount of veiling glare over the exposure field reduces the contrast of the quantum noise detected by the II. Except for the correction factor for the veiling-glare effect, this conversion method is similar to that achieved with the gradient of the H&D curve in the analysis of the noise Wiener spectrum of a screen–film system.[3]

IV. RESULTS

Figure 1 shows the characteristic curves (DSA pixel value versus log relative x-ray intensity) of our Digitron 2 system for images obtained with 256 × 256 and 512 × 512 matrix sizes. These curves are the averages of ten independently measured curves over several days, which were graphically superimposed and smoothed by eye. The exposures were made at 63 kV and at 2 frames/sec with the logarithmic amplifier. It is apparent that the characteristic curve is dependent on the matrix size, and that each curve tends to saturate at both high and low DSA numbers. It should be noted that the 256 × 256 matrix size image was obtained with a blanking interlaced mode during the TV camera readout, whereas the 512 × 512 matrix size image was obtained with a nonblanking progressive readout mode. We believe that the shapes of these curves depend on the properties of the logarithmic amplifier and other electronic components in the DSA unit, since the light output of the II is related linearly to the x-ray intensity incident on the II.[20,21] Therefore, the characteristic curve of the II–TV digital system is basically equal to the relationship between the light output of the II and the pixel value. We have confirmed that the shape of the curve does not vary with the II mode used. We also found that, for both matrix sizes, the characteristic curves of another Digitron 2 unit, recently installed, were similar to that for the 256 × 256 matrix size shown in Fig. 1.

In the initial stage of this study, images of the stepwedge were transferred from the Digitron 2 to a Siemens Evaluskop computer system in order to determine the DSA pixel values. However, we found that we could read within the experimental error the average DSA pixel values representing each area of the aluminum stepwedge by employing a windowing technique, i.e., by changing the window level, at the minimum window width, until one of the gray levels on the cathode ray tube (CRT) monitor matched the average gray level of the selected region in the stepwedge image. The window level corresponding to the matched gray level indicated the pixel value of the step. This windowing technique would be unnecessary if ROI (region of interest) software were available. In addition, we found that the variation of the characteristic curves obtained from different frames in the same exposure sequence was negligible except in the first few frames during which the exposure parameters were being adjusted by the automatic exposure control. Also, variations among curves obtained at different exposures and on different days were usually small, as illustrated in Fig. 1. Only a lateral shift of the curve along the relative x-ray intensity axis was observed.

Gradient curves for both matrix sizes are shown in Fig. 2.

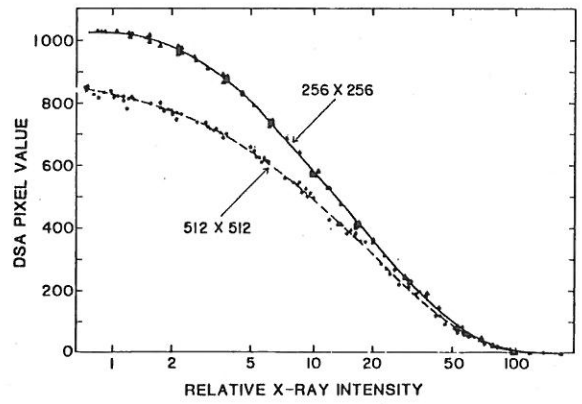

FIG. 1. Characteristic curves relating the pixel value to the relative x-ray intensity incident on a DSA system, for two matrix sizes. A logarithmic amplifier was employed before the A/D converter. The experimental data points were obtained from ten independent measurements.

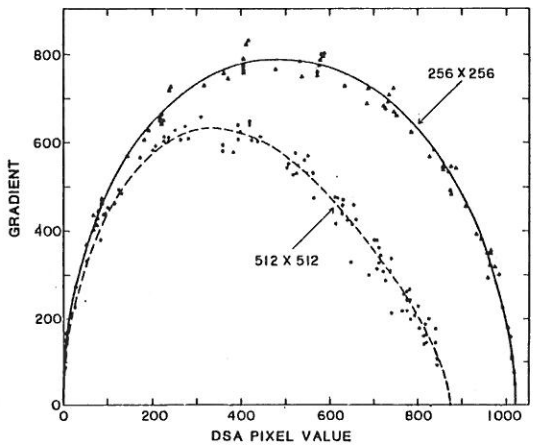

FIG. 2. Gradient curves for two matrix sizes, obtained from the slopes of the characteristic curves shown in Fig. 1.

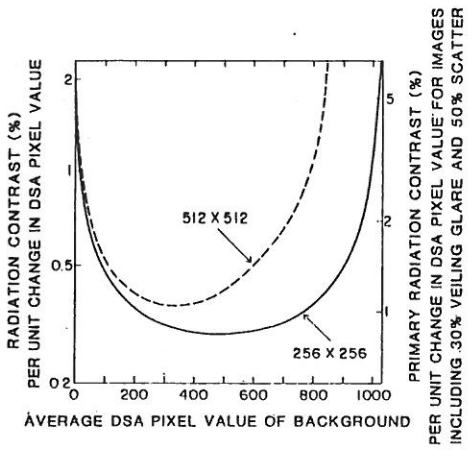

FIG. 3. Conversion factor of signal contrast from the DSA pixel value to the radiation contrast (left ordinate) was calculated from Eq. (2). The conversion factor on the right ordinate was calculated from Eq. (3) for a case including 50% scatter and 30% veiling glare.

Each curve is the average of ten gradient curves, each of which was calculated from a different fitted characteristic curve. The conversion factor of the signal contrast in terms of the DSA pixel value to that in terms of the radiation contrast was calculated from Eq. (2) and is plotted in Fig. 3 as a function of the average DSA pixel value of the background. In addition, the primary radiation contrast per unit change in DSA pixel value (for a signal component), which is calculated from Eq. (3), is plotted for the case in which 50% scatter and 30% veiling glare are included. Figure 3 indicates that, for our system, the signal contrast of one DSA pixel value corresponds to a primary radiation contrast of approximately 1%, when the average pixel value is in the mid-range and when 50% scatter and 30% veiling glare are included.

Figure 4 illustrates two characteristic curves, each obtained with the linear amplification mode for the 256 × 256 matrix size, but measured on two independent occasions. The solid curve is linear, whereas the dashed curve indicates a distorted response, which is probably due to an incorrect adjustment of the A/D converter and/or the amplifier. Occasionally, we observed changes in the shape of the characteristic curve that coincided with the malfunction of an electronic component in the power supply and with its repair. These results appear to indicate the usefulness of the characteristic-curve measurement for monitoring of the system response.

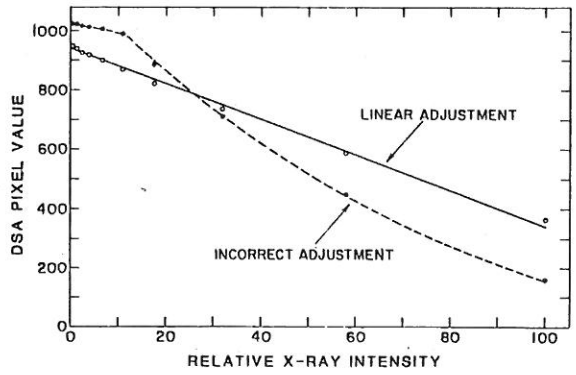

FIG. 4. Characteristic curves for the 256 × 256 matrix size in the linear amplifier mode, for the case of incorrect (dashed curve) and linear (solid curve) adjustments of the A/D converter and/or the amplifier.

V. DISCUSSION

A fundamental problem with the stepwedge method is that the x-ray beam qualities transmitted through each step of an aluminum stepwedge can differ substantially due to filtration. Consequently, the relative x-ray intensities transmitted through different steps, as measured by an image receptor (or detector), depend strongly on the x-ray energy absorption properties of the detector. This implies that the aluminum attenuation curve measured with an ionization chamber will generally not be the same as the curve measured with an image intensifier. In order to determine accurately the relative x-ray intensities detected under each step of the aluminum stepwedge by the image intensifier, one has to measure the x-ray intensities with a detector whose x-ray absorption characteristics are similar to those of the II and whose x-ray sensitometric relationship is known. Thus we chose three screen–film systems, Kodak Lanex Regular/OG, DuPont Cronex Quanta II/XL, and Cronex Quanta III/XL, as x-ray detectors. Since the relationship between the optical density and the relative x-ray intensity incident on a screen–film system (i.e., the H&D curve) can be determined accurately with an inverse-square intensity-scale x-ray sensitometer,[3–5] we can obtain the relative x-ray intensities detected under the stepwedge from the aluminum attenuation curves measured with these screen–film systems, as will be discussed later. It should be noted that we assumed the x-ray absorption characteristics of these screens to be similar to those of the II input phosphor (CsI). This assumption was verified by a computer simulation of attenuation curves with different detectors, which can be described as follows. We calculated the attenuation curves of alumi-

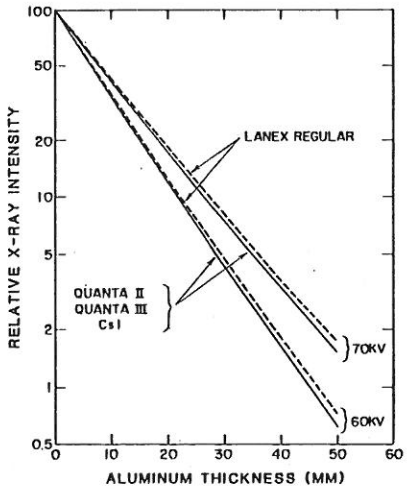

FIG. 5. Calculated attenuation curves for aluminum with three different screens and with CsI phosphor (100 mg/cm^2) at 60 and 70 kV with a 0.81-mm copper filter. Screens used were Lanex Regular (Gd_2O_2S; 130 mg/cm^2), Quanta II (BaFCl; 85 mg/cm^2), and Quanta III (LaOBr; 108 mg/cm^2).

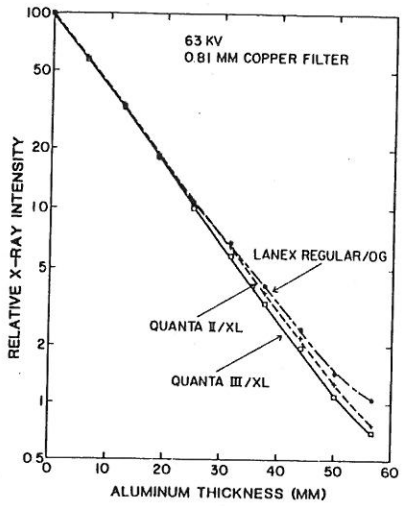

FIG. 6. Measured attenuation curves for aluminum, obtained with three screen–film systems at 63 kV.

num, obtained with the above three screens and with a CsI phosphor, for two incident spectra at 60 kV [half-value layer (HVL): 2.30 mm Al] and 70 kV (HVL: 2.65 mm Al) by taking into account the screen absorption of the primary x rays and the reabsorption of the K x rays in the phosphor.[29] The coating density of the CsI phosphor was assumed to be 100 mg/cm^2. As shown in Fig. 5, the attenuation curve obtained with the CsI phosphor is in good agreement with the curves calculated for the Quanta II and the Quanta III screens. This result may be related to the fact that the K edges (Cs: 36.0 keV; I: 33.2 keV) of CsI are very close to the K edges (Ba: 37.4 keV; La: 39.0 keV) of the high atomic number elements contained in these screen phosphors. However, the attenuation curve calculated for the Lanex Regular screens is slightly higher than those obtained with the other screens; this result is probably due to the high K edge of Gd (50.2 keV) contained in the Lanex Regular phosphor.

Figure 6 shows the measured attenuation curves of the aluminum stepwedge for the three screen–film systems. Each curve represents the average of at least three independent measurements. In this experiment, a 2× magnification technique at a 100-cm focal-spot–film distance, together with a 12:1, 57 lines/cm grid, was used for elimination of the scattered radiation. The curves were measured at a beam quality of 63 kV, with added filtration of 0.81-mm-thick copper. In addition, the x-ray field was collimated to the area of the stepwedge to reduce the off-focus radiation. The relative x-ray intensities detected under the aluminum stepwedge were determined from the optical density values by use of the corresponding H&D curve of each screen–film system. The field nonuniformity of the x-ray intensity was corrected. The curves are almost linear on the semilog plot, especially those for the Quanta II and Quanta III screens. These curves agree well within the experimental errors at the thin portion of the aluminum and differ slightly in the region with thick aluminum. The curve obtained with Lanex Regular screens is slightly above the other curves, as was also observed from the calculated values. These results thus appear to support our assumption that the energy response of the CsI phosphor is similar to those of the Quanta II and Quanta III screens.

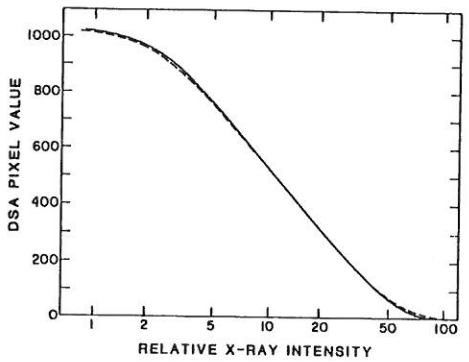

FIG. 7. Comparison of characteristic curves with (dashed curve) and without (solid curve) correction for the nonuniformities of the II response and the incident x-ray intensity, obtained for the 256 × 256 matrix size and the 17-cm II mode.

Therefore, for the abscissa of the characteristic curve for the DSA system, we determined the relative x-ray intensities detected under the stepwedge from the average of the attenuation curves obtained with the Quanta II and Quanta III screens.

The effect of spatial nonuniformities in the II–TV response[23,25] and in the x-ray beam incident on the II (e.g., due to the heel effect) on the measured characteristic curve was corrected by obtaining an image without the aluminum stepwedge. The characteristic curves with and without the correction for the nonuniformities are shown in Fig. 7, in which it is apparent that the change in the curve due to the nonuniformity correction is within the experimental error. Thus, a correction for nonuniformity appears to be unnecessary in measurements of the characteristic curve of our DSA system.

To demonstrate the validity of the measured characteristic curve, we determined the attenuation curves of iodine at three different exposure levels. We constructed an iodine phantom that contained individual compartments whose iodine content ranged from 0 to 100 mg/cm^2. This phantom, together with a 12-cm-thick Lucite block, was imaged by the Digitron 2 with a 256 × 256 matrix at 63 kV and with a

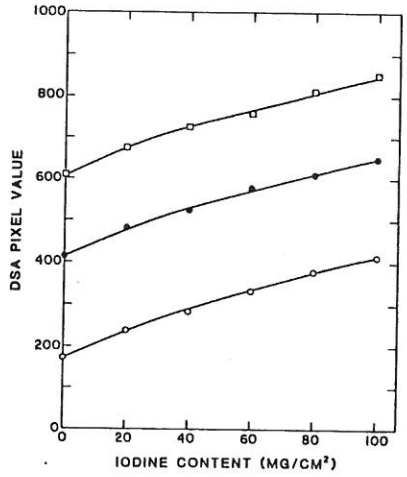

FIG. 8. Relationship between DSA pixel values and iodine content, measured at three different exposure levels for the 256 × 256 matrix size.

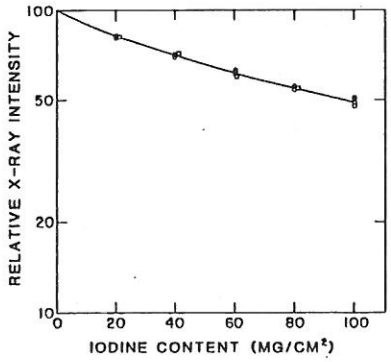

FIG. 9. Attenuation curve of iodine, obtained at three different exposure levels.

broad-beam geometry. Three independent images at different exposure levels were obtained by fooling the automatic exposure control of the system, as described earlier. The curves in Fig. 8 indicate different relationships between the DSA pixel value and the iodine content. However, when the DSA pixel values were converted to relative x-ray intensities by means of the characteristic curve (this corresponds to "linearization" of the DSA system response), the attenuation curves for iodine obtained at different exposure levels coincided within the experimental error, as shown in Fig. 9. This result seems to indicate that the DSA system can be linearized with the use of the characteristic curve for quantitative image analysis, and also to verify that the measured characteristic curve can be useful in relating the pixel value to the relative x-ray intensity incident on the II–TV system.

In conventional screen–film radiography, the optical density is commonly considered to be the output of the system response in the determination of the characteristic curve of the system. In this study, however, we employed the pixel value as the output of a DSA system, excluding the effect of a multiformat camera and photographic film. This is because the pixel value is a unique output of a digital imaging system, which can be subjected to quantitative analysis of image data. For visualization of digital-image data on a film, however, the optical density needs to be considered as the system output, which can be determined by incorporating the relationship between the optical density and the pixel value into the characteristic curve defined in this study.

VI. CONCLUSION

We developed a simple method for determining the characteristic curve of II–TV digital systems. The gradient curve of the system was obtained from the slope of the characteristic curve. Measurements of the characteristic curve will be useful for monitoring of the DSA system response as well as for quantitative determination of basic imaging properties such as the radiation contrast,[30–32] the MTF,[33] and the noise Wiener spectrum.[28]

ACKNOWLEDGMENTS

The authors thank K. Ohara for his discussions, M. Carlin for his technical assistance, E. Lanzl for editing the manuscript, and E. Ruzich for her secretarial assistance. This work was supported by USPHS Grant CA 24806.

[a] Presented in part at the 70th Scientific Assembly and Annual Meeting of the Radiological Society of North America, Washington, DC, 25–30 November 1984.

[1] C. E. Metz and K. Doi, Phys. Med. Biol. **24**, 1079 (1979).
[2] *The Physics of Medical Imaging: Recording System Measurements and Techniques*, edited by A. G. Haus (American Institute of Physics, New York, 1979).
[3] K. Doi, G. Holje, L.-N. Loo, H.-P. Chan, J. M. Sandrik, R. J. Jennings, and R. F. Wagner, HHS Pub. (FDA) 82-8187 (1982).
[4] A. G. Haus and K. Rossmann, Radiology **94**, 673 (1970).
[5] A. G. Haus, K. Rossmann, C. J. Vyborny, P. B. Hoffer, and K. Doi, J. Appl. Photogr. Eng. **3**, 114 (1977).
[6] J. Hale and P. Bloch, Radiology **128**, 820 (1978).
[7] D. R. Bednarek and S. Rudin, Proc. Soc. Photo-Opt. Instrum. Eng. **233**, 2 (1980).
[8] M. V. Yester, G. T. Barnes, and M. A. King, Radiology **136**, 785 (1980).
[9] L. K. Wagner, G. T. Barnes, J. A. Bencomo, and A. G. Haus, Med. Phys. **10**, 365 (1983).
[10] B. A. Arnold, Proc. Soc. Photo-Opt. Instrum. Eng. **347**, 7 (1982).
[11] *Recent Developments in Digital Imaging*, edited by K. Doi, L. Lanzl, and P.-J. P. Lin (American Institute of Physics, New York, 1985).
[12] W. R. Brody, *Digital Radiography* (Raven, New York, 1984).
[13] S. J. Riederer and R. A. Kruger, Radiology **147**, 633 (1983).
[14] R. A. Kruger and S. J. Riederer, *Basic Concepts of Digital Subtraction Angiography* (Hall, Boston, 1984).
[15] F. A. DiBianca, F. J. Kohout, R. H. Propst, P. F. Jaques, and B. G. Thompson, Proc. Soc. Photo-Opt. Instrum. Eng. **347**, 14 (1982).
[16] C. G. Shaw and D. A. Bassano, Proc. Soc. Photo-Opt. Instrum. Eng. **347**, 24 (1982).
[17] C. G. Shaw, D. A. Bassano, and Z. D. Grossman, Proc. Soc. Photo-Opt. Instrum. Eng. **347**, 122 (1982).
[18] G. T. Barnes, R. A. Sones, and M. M. Tesic, Radiology **154**, 801 (1985).
[19] W. J. MacIntyre, W. Pavlicek, J. H. Gallagher, T. F. Meaney, E. Buonocore, and M. A. Weinstein, Radiology **139**, 307 (1981).
[20] G. Cohen, L. K. Wagner, and E. N. Rauschkolb, Radiology **144**, 613 (1982).
[21] J. A. Seibert, O. Nalcioglu, and W. W. Roeck, Med. Phys. **11**, 172 (1984).
[22] R. B. Wilsey, Am. J. Roentgenol. **8**, 328 (1921).
[23] C. A. Mistretta, in *The Physics of Medical Imaging: Recording System Measurements and Techniques*, edited by A. G. Haus (American Institute of Physics, New York, 1979), p. 182.
[24] S. J. Riederer, B. F. Belander, G. S. Keyes, and N. J. Pelc, Proc. Soc. Photo-Opt. Instrum. Eng. **314**, 132 (1981).
[25] H. Roehring and T.-Y. Fu, in *Recent Developments in Digital Imaging*, edited by K. Doi, L. Lanzl, and P.-J. P. Lin (American Institute of Physics, New York, 1985), p. 82.
[26] Y. Higashida, K. Doi, J. L. Lehr, and H. MacMahon, Med. Phys. **11**, 646 (1984).
[27] H.-P. Chan and K. Doi, Phys. Med. Biol. **28**, 109 (1983).
[28] M. Lissak Giger, K. Doi, and H. Fujita, Med. Phys. **11**, 385 (1984) (Abstract).
[29] H.-P. Chan and K. Doi, Phys. Med. Biol. **28**, 565 (1983).
[30] H. Fujita, K. Doi, H.-P. Chan, and M. Lissak Giger, in *Recent Developments in Digital Imaging*, edited by K. Doi, L. Lanzl, and P.-J. P. Lin (American Institute of Physics, New York, 1985), p. 566.
[31] H. Fujita, K. Doi, H.-P. Chan, M. Lissak Giger, and E. E. Duda, Radiology **155**, 799 (1985).
[32] K. Ohara, K. Doi, M. Lissak Giger, H. Fujita, H.-P. Chan, and C. E. Metz, Radiology **153(P)**, 318 (1984) (Abstract).
[33] H. Fujita, K. Doi, and M. Lissak Giger, Med. Phys. **12**, 713 (1985).